High-frequency sensor data capture short-term variability in Fe and Mn cycling due to hypolimnetic oxygenation and seasonal dynamics in a drinking water reservoir

Nicholas W. Hammond

Affiliation: Department of Geosciences, Virginia Tech
Email: hammondnw@vt.edu

ORCID ID: 0000-0003-2975-8280

François Birgand

Affiliation: Department of Biological and Agricultural Engineering

Email: birgand@ncsu.edu

ORCID ID: 0000-0002-5366-1166

Cayelan C. Carey

Affiliation: Department of Biological Sciences, Virginia Tech
Email: cayelan@vt.edu

ORCID ID: 0000-0001-8835-4476

Bethany Bookout

Affiliation: Department of Biological Sciences, Virginia Tech

Email: youthoutreach@newriverlandtrust.org

ORCID ID: 0000-0001-8394-926X

Adrienne Breef-Pilz

Affiliation: Department of Biological Sciences, Virginia Tech

Email: abreefpilz@vt.edu

ORCID ID: 0000-0002-6759-0063

Madeline E. Schreiber

Affiliation: Department of Geosciences, Virginia Tech

Email: mschreib@vt.edu

ORCID ID: 0000-0002-1858-7730

Authorship Statement

NWH, FB, and MES co-conceived the design of the study. NWH led field sampling, and MES, BB, and ABP assisted in field sampling. FB, CCC, and BB conducted the initial field testing for the MUX and development of the PLSR analysis workflow. ABP led the collection of auxiliary sensor data. FB, CCC, and MES contributed to conceptual development, which substantially improved the quality of the manuscript.

Abstract

The biogeochemical cycles of iron (Fe) and manganese (Mn) in lakes and reservoirs have predictable seasonal trends, largely governed by stratification dynamics and redox conditions in the hypolimnion. However, short-term (i.e., sub-weekly) trends in Fe and Mn cycling are less well-understood, as most monitoring efforts focus on longer-term (i.e., monthly to yearly) time scales. The potential for elevated Fe and Mn to degrade water quality and impact ecosystem functioning, coupled with increasing evidence for high spatiotemporal variability in other biogeochemical cycles, necessitates a closer evaluation of the short-term Fe and Mn cycling dynamics in lakes and reservoirs. We adapted a UV-visible spectrophotometer coupled with a multiplexor pumping system and PLSR modeling to generate high spatiotemporal resolution predictions of Fe and Mn concentrations in a drinking water reservoir (Falling Creek Reservoir, Vinton, VA, USA) equipped with a hypolimnetic oxygenation (HOx) system. We quantified hourly Fe and Mn concentrations during two distinct transitional periods: reservoir turnover (Fall 2020) and initiation of the HOx system (Summer 2021). Our sensor system was able to successfully predict mean Fe and Mn concentrations as well as capture sub-weekly variability, ground-truthed by traditional grab sampling and laboratory analysis. During fall turnover, hypolimnetic Fe and Mn concentrations began to decrease more than two weeks before complete mixing of the reservoir occurred, with rapid equalization of epilimnetic and hypolimnetic Fe and Mn concentrations in less than 48 hours after full water column mixing. During the initiation of hypolimnetic oxygenation in Summer 2021, we observed that Fe and Mn were similarly affected by physical mixing in the hypolimnion, but displayed distinctly different responses to oxygenation, as indicated by the rapid oxidation of soluble Fe but not soluble Mn. This study demonstrates that Fe and Mn concentrations are highly sensitive to shifting DO and stratification and that their dynamics can substantially change on hourly to daily time scales in response to these transitions.

Keywords: Hypolimnetic Oxygenation, Iron, Manganese, Spatiotemporal resolution, Spectrophotometer, Turnover

Highlights:

- We used UV-vis spectral data and PLSR to quantify Fe and Mn in a reservoir
- High-resolution predictions in time and depth were made during fall turnover and summer oxygenation
- Fe and Mn concentrations are highly sensitive to DO and stratification
- Fe and Mn dynamics can shift on hourly to daily time scales
- Our sensor approach holds much promise for drinking water monitoring of metals

1. Introduction

Elevated levels of iron (Fe) and manganese (Mn) in lakes and reservoirs have negative consequences for ecosystem health and water quality. Increasing Fe concentrations have been linked to the long-term browning of lakes, which has numerous, significant ecological consequences (Kritzberg et al. 2020). Mn contamination of drinking water can pose serious risks to human health, especially in children (Wasserman et al. 2006). Furthermore, high concentrations of both metals negatively affect the taste, odor, and appearance of water and can damage water supply infrastructure through corrosion and deposition (World Health Organization 2017). As a result, the U.S. Environmental Protection Agency (EPA) has established secondary standards for Fe and Mn concentrations in drinking water of 0.3 and 0.05 mg/L, respectively (EPA 2021).

As Fe and Mn are redox-sensitive elements, their abundance in aquatic systems is largely influenced by dissolved oxygen (DO) concentrations (Hem 1972, Davison 1993). The oxidation state of Fe and Mn in natural waters is dominated by two forms: insoluble, oxidized Fe(III) and Mn(IV), and soluble, reduced Fe(II) and Mn(II) (Davison 1993). In most aquatic systems under circumneutral pH, this oxidation state is determined by the redox conditions at a given point in space and time. Under oxic conditions, Fe and Mn are generally present as insoluble Fe(III) and Mn(IV) solids in rocks and sediments. However, thermal stratification in lakes and reservoirs can create anoxic conditions in the hypolimnion and bottom sediments, promoting the microbial reduction of Fe and Mn in sediments and the subsequent release of soluble, reduced Fe and Mn into the water column (Lovely 1991). In such settings, soluble Fe and Mn can accumulate in hypolimnetic waters throughout the stratified period (McMahon 1969, Davison 1993, Beutel et al. 2008, Munger et al. 2016, Krueger et al. 2020).

An increasingly used *in situ* approach for mitigating high Fe and Mn in drinking water reservoirs is hypolimnetic oxygenation (HOx), which creates oxic conditions in previously anoxic waters and creates a thicker aerobic zone in bottom sediments (e.g., Beutel and Horne 1999, Bryant et al. 2011, Dent et al. 2014, Gantzer et al. 2009, Gerling et al. 2014). By increasing oxygen availability in the hypolimnion, HOx operation hinders the release of soluble Fe and Mn into sediment pore waters, slows upward diffusion into the water column, and promotes Fe and Mn oxidation and precipitation in the hypolimnion (Preece et al. 2019). HOx systems have been shown to effectively reduce soluble Fe and Mn in the hypolimnion of drinking water reservoirs (Gantzer et al. 2009, Bryant et al. 2011). However, removing soluble Mn from the water column requires more sustained oxygen inputs, due to its slower oxidation reaction kinetics (Bryant et al. 2011, Munger et al. 2016). To optimize water treatment using HOx systems, it is essential for drinking water managers to understand both the short-term (sub-weekly) and long-term (monthly to yearly) dynamics of Fe and Mn cycling in supply reservoirs.

Although Fe and Mn cycling in temperate lakes and reservoirs has predictable seasonal trends dictated by thermal stratification, there is a lack of research on short-term Fe and Mn dynamics. Quantifying short-term trends requires

high-frequency data, which we define as having a temporal resolution of daily or shorter. To our knowledge, there is no standard definition for classifying data as 'high-frequency' or trends as 'short-term.' Thus, we developed operational definitions based on the contrast with traditional monitoring frequencies, which are typically weekly or longer (e.g., Marcé et al. 2016). The paucity of previous research on Fe and Mn cycling at sub-weekly scales represents a key knowledge gap, given that biogeochemical process rates can fluctuate rapidly over hourly to daily time scales (McClain et al. 2003). Studies have identified diel signals in the cycles of numerous biogeochemical variables, including Fe and Mn, and many biological and chemical processes in aquatic environments operate on hourly to daily scales, often with significant impacts on nutrient cycling and ecosystem productivity (Istvánovics, Osztoics, & Honti 2004, Nimick, Gammons, & Parker 2011, Kurz et al. 2013). Additionally, episodic hydrologic events, which may be missed by traditional sampling methods, can have pronounced effects on biogeochemical cycling dynamics (e.g., Marcé et al. 2016, Coraggio et al. 2022).

Studies analyzing the efficacy of HOx systems have observed substantial changes in Fe and Mn concentrations in response to changes in DO concentrations (Dent et al. 2014, Munger et al. 2019). For example, Dent et al. (2014) found that total Fe and Mn concentrations decreased by 71% and 73%, respectively, after 8 hours of oxygenation of a previously-anoxic reservoir hypolimnion. Conversely, Munger et al. (2019) found that Fe and Mn sediment fluxes into the water column were 1.4 and 4.5 times higher, respectively, two weeks after the onset of hypolimnetic anoxia in a reservoir. The dynamic behavior of Fe and Mn concentrations in response to both management and natural processes (e.g., seasonal thermal stratification) underscores the importance of quantifying these complex cycling dynamics, which could have substantial implications for drinking water management and water quality monitoring. To date, monitoring programs have been hindered by the coarse temporal frequency of months to seasons necessitated by traditional manual sampling and laboratory analysis techniques.

Recent developments in sensor technology have enabled high-frequency collection of some water quality variables *in situ*, without the need for manual sampling and laboratory analysis (Porter et al. 2009, Rode et al. 2016, Kruse 2018). However, most high-frequency sensors are only capable of measuring a single variable at a time and typically have a low spatial resolution. Moreover, numerous water quality variables, including Fe and Mn, lack instrumentation capable of unattended, reagent-less, high-frequency measurement.

To circumvent the limitations of current sensor technology, spectrophotometers have been designed to measure water quality variables *in situ* at a high frequency using multi-wavelength absorbance patterns in the ultraviolet-visible (UV-vis) spectrum. These sensors do not require chemical reagents and are capable of measuring multiple variables simultaneously. To date, UV-vis spectrophotometers have been successfully used to measure chemical variables that have a strong correlation with known peaks in their absorbance spectra, such as nitrate and dissolved organic carbon (DOC) (Etheridge et al. 2014, Sakamoto, Johnson,

& Coletti 2009). Additionally, several studies have had success using them to measure concentrations of other biogeochemical variables without well-defined spectral peaks, such as Fe, total phosphorus (TP), soluble reactive phosphorus (SRP), and dissolved silica (Si) (Birgand et al. 2016, Etheridge et al. 2014, Vaughan et al. 2018). Although Fe and Mn are not known to have well-defined spectral peaks, they absorb and scatter light at wavelengths across the UV-vis spectrum and they can affect the absorbance of a water sample through complexation with organic molecules (Poulin et al. 2014, Weishaar et al. 2003, Xiao et al. 2013). Therefore, the covariance between the variable of interest (e.g., Fe or Mn) and the overall "color matrix" of the water (the combination of multiple light-sensitive proxies) can be detected in the UV-vis absorbance spectra and used to predict concentrations of the variable of interest with statistical algorithms (Birgand et al. 2016). Laboratory-measured concentrations from manually collected samples are then subsequently used to develop predictive models that correlate known concentrations with absorbance spectra.

Numerous algorithms exist for calibrating UV-vis absorbance spectra to observed concentrations, but the most commonly-employed method is partial least squares regression (PLSR) (DiFoggio 2000, Birgand et al. 2016, Vaughan et al. 2018). PLSR is well-suited for modeling relationships within data that have a large number of highly correlated explanatory variables and relatively few observations, such as multi-wavelength spectral measurements (Wold et al. 2001). Previous studies have used *in situ* spectrophotometers and PLSR models to predict water quality variables in a variety of environments, including streams, lakes, estuaries, and oceans, with varying levels of predictive accuracy (Sakamoto, Johnson, & Coletti 2009, Avagyan, Runkle, & Kutzbach 2014, Etheridge et al. 2014, Birgand et al. 2016, Vaughan et al. 2018). However, to the best of our knowledge, only one study (Birgand et al. 2016) has evaluated the potential of this method to observe the high-frequency dynamics of metals in lakes and reservoirs.

Because the application of this method is relatively new, only a few studies have attempted to quantify the uncertainty of water chemistry predictions made using PLSR and spectrophotometric data (Bieroza & Heathwaite 2016, Vaughan et al. 2018). Uncertainty quantification is crucial for determining the accuracy and feasibility of these methods, especially in natural waters that have a complex chemical composition with an unknown relationship to the measured spectrophotometric color matrix (Bieroza & Heathwaite 2016; Rieger, Langergraber, & Siegrist 2006; Vaughan et al. 2018). Furthermore, the ability of a PLSR model to make accurate predictions is contingent upon how well the training data capture the variability in predicted concentrations, which in turn influences the generalizability of the model (Wold et al. 2001, DiFoggio 2000). In addition to these factors, photometric noise (i.e., random differences in spectral measurements) and spectral artifacts (e.g., instrument drift and fouling) can introduce error into model predictions (DiFoggio 2000).

Thus, *in situ* spectrophotometer data coupled to PLSR modeling potentially

offer useful insight on rapidly changing metals concentrations in reservoirs and lakes. However, because of strong thermal gradients with depth in lakes, a single spectrophotometer cannot capture metals concentrations that may also rapidly change with depth. Additionally, the cost of *in situ* spectrophotometers ($8000-25000 USD as of 2022) prohibits the acquisition of many needed to characterize spatial dynamics as well. For this reason, Birgand et al. (2016) designed a multiplexed sequential sampling system to pump water from different depths at one site to one spectrophotometer used as a portable lab above the water's surface. This system has proven to be able to characterize variable reservoir biogeochemical concentrations over both depth and time (Birgand et al., 2016).

Motivation and objectives

We used an *in situ* spectrophotometer coupled with a multiplexor pumping system and PLSR modeling to predict high-frequency Fe and Mn concentrations at multiple depths in a seasonally-stratified drinking water reservoir. We then used this approach to observe the short-term (sub-weekly) variability of Fe and Mn cycling during two distinct transitional periods: reservoir turnover in Fall 2020 and initiation of HOx operation in Summer 2021. The objectives of this study were to: 1) assess the accuracy and uncertainty associated with predictions of Fe and Mn concentrations using spectral absorbance data coupled with PLSR modeling, 2) identify whether Fe and Mn cycling dynamics exhibit temporal variability across depth gradients, and 3) quantify the effects of reservoir turnover and hypolimnetic oxygenation on Fe and Mn concentrations.

2. Methods

Study site

Field data were collected at Falling Creek Reservoir (FCR), a small (0.12 km^2, maximum depth = 9.3 m), dimictic reservoir located in Vinton, Virginia, USA (Figure 1, Gerling et al. 2014). FCR was constructed in 1898 and is managed as a drinking water reservoir by the Western Virginia Water Authority (WVWA) in Roanoke, VA. The summer stratified period at FCR typically lasts from May to October. FCR is located in a forested catchment with one primary inflow and several smaller tributaries. Due to the underlying geology, which consists of Fe- and Mn-rich rocks of the Blue Ridge and Piedmont Provinces (Woodward, 1932), this region has elevated Fe and Mn concentrations in surface and groundwater (Chapman et al. 2013).

FCR contains a HOx system, which can be activated and deactivated to control DO concentrations in the hypolimnion without altering thermal stratification or water temperature (Figure 1, Gerling et al. 2014). The HOx system at FCR was activated from 29 June 2020 until 2 December 2020, when it was turned off for the winter period. It remained deactivated from 2 December 2020 until 11 June 2021, at which point it was turned back on and remained activated until the end of the study period on 21 June 2021.

FCR is equipped with sensors that continuously monitor the physical, chem-

ical, and meteorological conditions at the reservoir's deepest spot, which was the primary sampling location in this study (Figure 1). DO sensor data was collected using a YSI EXO2 (Yellow Springs, OH) deployed at 1.6m and two In-Situ RDO-PRO-X sensors (Fort Collins, CO) at 5m and 9m (Carey et al. 2022b). Ten-minute resolution temperature measurements were collected by *in situ* sensors deployed every meter from the surface to the reservoir sediments (Carey et al. 2022b). To quantify the intensity of reservoir thermal stratification during each deployment, we calculated Schmidt stability (J m^{-2}, Idso 1973) using temperature measurements and bathymetric data from FCR (Carey et al. 2022c) as inputs to the R package *rLakeAnalyzer* (Winslow et al. 2019). Meteorological variables were measured by a research-grade Campbell Scientific meteorological station deployed on the dam of FCR (Carey et al. 2022a).

High-Frequency Monitoring System

We monitored high-frequency light absorbance at multiple depths in FCR using a s::can Spectrolyser UV-Visible spectrophotometer (s::can Messtechnik GmbH, Vienna, Austria). This spectrophotometer was coupled with a multiplexor pumping system ('MUX' from MultiplexÔ, LLC; for technical details on the multiplexor pumping system and the sensor setup, refer to Birgand et al. 2016 and Figures S1-S3). The MUX pumps water samples from multiple depths into a flow-through cuvette where the UV-vis absorbance spectra of the sample are measured by the spectrophotometer. The system used in our study collected measurements of light absorbance every 2.5 nm wavelengths from 200 nm to 732.5 nm (optical path length of 10 mm) approximately at an hourly time step for six monitoring depths in the reservoir.

The MUX system was used to collect high-frequency data during two time periods: reservoir turnover ("Turnover Deployment") and the initiation of HOx operation ("Oxygen On Deployment"). The Turnover Deployment captured the natural oxygenation and mixing processes that occurred during reservoir turnover and lasted from 16 October to 9 November 2020. In this study, fall turnover was defined as the first time when the temperature differential between 0.1 m and 9 m depths in the reservoir was <1 °C after summer stratification (following McClure et al. 2018), which occurred on 2 November 2020. During this time period the HOx system was on, so the hypolimnion was oxic before turnover, but the reservoir was thermally stratified. The Oxygen On Deployment was conducted between 26 May and 21 June 2021; during that time the HOx system was initiated on 11 June 2021 at 11:00 EDT. This deployment captured the engineered oxygenation and mixing processes resulting from the initiation of HOx operation. The reservoir was thermally-stratified and the hypolimnion was anoxic (DO < 1 mg/L) prior to HOx operation and thus, while HOx operation added oxygen to the hypolimnion, we observed a limited increase in DO concentrations due to high chemical oxygen demand. The HOx system induced internal mixing within the hypolimnion, but the overall thermal stratification of the reservoir was not affected.

We took multiple steps to limit the influence of fouling of the internal compo-

nents of the MUX system, due to precipitation of Fe in contact with oxygen in the measuring cuvette. Between each pump cycle, deionized water was flushed through the system. At the end of each pump sequence (one sample from each depth), dilute hydrochloric acid (5%) was automatically pumped through the system and allowed to sit in the flow-through cuvette for approximately 2 minutes. We also collected a reference measurement in air at the end of each cycle, which was useful in determining the extent of fouling. Despite these efforts, some fouling was still evident during certain time periods (see Figures S4-5). Fouling was most pronounced in the lower wavelengths (200-250 nm; see Figures S6-7) and therefore we removed values for wavelengths less than 250 nm before fitting PLSR models.

Sampling Methods

As part of an ongoing monitoring program, we sample total and soluble Fe and Mn weekly throughout the stratified period. For this study, water samples were collected at the reservoir outtake depths of 0.1, 1.6, 3.8 m (epilimnion), 5.0 m (metalimnion), 6.2, 8.0, and 9.0 m (hypolimnion) using a 4-L Van Dorn sampler, thereby matching the MUX sampling depths. Samples for soluble Fe and Mn were syringe-filtered using 0.45 µm nylon filters. Both total and soluble metals samples were preserved with trace metal grade nitric acid to pH < 2. Samples were analyzed using Inductively Coupled Plasma Mass Spectrometry (ICPMS). Minimum reporting levels were 0.005 mg/L (Fe) and 0.0001 mg/L (Mn). The dataset, including methods for sample collection and analysis, can be found in Schreiber et al. (2022).

To assess short-term variability in metals concentrations and to calibrate and validate PLSR models, additional samples were collected every 2-4 hours during two 24-hour campaigns. The first campaign occurred on 16-17 October 2020 (n=7; Figure S8); the second campaign occurred on 10-11 June 2021 (n=8; Figure S9). All sampling data (weekly and high-frequency) were used to calibrate PLSR models.

Predicting Fe and Mn concentrations from optical measurements using PLSR

We used PLSR to compute predictions of total and soluble Fe and Mn concentrations based on the correlation between absorbance spectra and sampling data. Data analysis and QA/QC was performed in the R programming environment (R.v.4.2.1). Model building was conducted using the *pls* package (Mevik et al. 2020; R Core Team 2022), as described in Supplementary Information 1.1.

Separate PLSR models were developed for each variable (total Fe, soluble Fe, total Mn, and soluble Mn) and deployment. Based on the distinctly different chemical and biological characteristics between layers of the reservoir (i.e., epilimnion and hypolimnion), we found that the best fit was obtained when we used different models for the two layers. In stratified reservoirs such as FCR, Fe and Mn concentrations are much higher in the hypolimnion than the epilimnion. Therefore, we had an epilimnion model which included data from 0.1, 1.6, and 3.8 m and a hypolimnion model which included data from 6.2, 8.0, and

9.0 m (Table 1). Although we also collected data from 5.0 m, we did not include them in our analyses since this is at the transition between the two layers (metalimnion; see McClure et al. 2018) and thus not applicable to either layer. We developed separate models for the Turnover Deployment and the Oxygen On Deployment. In the end, we had four separate models for each of the four variables (total and soluble Fe and Mn), resulting in 16 different models.

To assess the uncertainty of the predictions made using PLSR, we calculated nonparametric bootstrap predictive intervals following methods described by Denham (1997) and reported in Supplementary Information 1.2. Model skill was assessed using the coefficient of determination (R^2) from the linear regression between predicted and observed values, as well as the root mean squared error of prediction (RMSEP) for each model (following Wold et al. 2001 and Mevik et al. 2020).

All observational data, including the spectrophotometer data, are published in the Environmental Data Initiative repository (Carey et al. 2022a, Carey et al. 2022b, Carey et al. 2022c, Schreiber et al. 2022, and Hammond et al. 2022). All code used to analyze the spectrophotometer data with PLSR and generate the figures is available in the Zenodo repository (Hammond 2022).

3. Results

3.1 *Routine Fe and Mn sampling trends*

Weekly sampling at FCR showed levels of Fe and Mn in exceedance of the EPA standards during the 2020 and 2021 stratified periods, with maximum total Fe and Mn concentrations of 18.5 mg/L and 2.2 mg/L, respectively (Figure 2). Hypolimnetic concentrations of both metals generally increased throughout the summer stratified period of each year, until reservoir fall turnover (Figure 2). Following reservoir turnover, concentrations of both metals remained low (< 1 mg/L) until the following spring. HOx activation from 11 June until 02 December in 2020 resulted in substantially lower hypolimnetic total Fe but not total Mn concentrations (Figure 2).

3.2 *PLSR Model Performance*

A comparison of skill metrics among the 16 models revealed that PLSR performed best for models calibrated with higher Fe and Mn concentrations that exhibited a larger standard deviation (Tables 1, S1; Figure S10). Model skill was also sensitive to the number of components included in each model. For the Turnover Deployment, the number of components included in the PLSR models ranged from 3-5 (9-14% of n). For the Oxygen On Deployment, 4 components were used for all PLSR models (8-9% of n) (Table 1). Sample size was negatively correlated with R^2, but positively correlated with RMSEP (Figure S10).

Turnover Deployment models explained a high proportion of the variability in total and soluble Fe and Mn concentrations, excluding hypolimnetic soluble Fe which had a poor model fit ($R^2 = 0.06$), due to extremely low concentrations

(median = 0.02 mg/L) during this time period (Table 1; Figure 3). In comparison, Oxygen On Deployment models explained a lower proportion of the variability in total and soluble Fe and Mn concentrations, despite having larger sample sizes for calibration (Table 1). In particular, PLSR model performance for total and soluble Mn was notably lower for the Oxygen On Deployment than for the Turnover Deployment (Tables 1, S1). PLSR model performance also varied between the hypolimnion and epilimnion. For most models, the epilimnetic PLSR model had a higher R^2 value than the corresponding hypolimnetic PLSR model (Table 1).

In most cases, PLSR predictions were within the range of concentration values in the calibration dataset (Figures 3, S11-12), but they did not capture some of the high-magnitude fluctuations in the sampling data. Analysis of the Fe and Mn time series (Figures 4D-E and 5D-E) and calibration (Figures S11-12) suggests that inaccuracy in the models was largely attributed to high calibration error for observations far from the mean concentration of the calibration data (i.e., outliers). Additionally, when predicting variables with relatively low concentrations (< 1 mg/L), especially with the epilimnion models, some predictions were in the negative range (Figures 4D-E; 5D-E).

3.3 *Reservoir Turnover Deployment*

3.3.1 Water Temperature, Stratification, and DO Concentrations

DO concentrations, water temperature, and Schmidt stability varied considerably over the course of the Turnover Deployment (Figures 4A-C). Prior to turnover, DO concentrations were strongly stratified by depth and exhibited large sub-daily fluctuations in the epilimnion and metalimnion (Figure 4C). Hypolimnetic DO concentrations were stable around 2 mg/L during the pre-turnover period, due to the HOx system operation (Figure 4C). A sharp temperature gradient (4-7°C) between the epilimnion and hypolimnion existed until approximately 3 days prior to turnover (Figure 4B). However, the water temperature profile equalized periodically between the metalimnion and hypolimnion prior to turnover, indicating ephemeral periods of mixing between those layers (Figure 4B). Starting on 29 October 2020, the temperature gradient decreased progressively until the full water column temperature profile equalized on 02 November 2020, meeting our criteria for turnover.

3.3.2 Predicted Fe and Mn Concentrations

Reservoir turnover had substantial impacts on Fe and Mn concentrations. At the beginning of the deployment (16 October 2020), 17 days prior to turnover, both Fe and Mn displayed large differences in concentration between the epilimnion and hypolimnion (Figures 4D-E). The average total Fe and total Mn concentrations across all hypolimnetic depths (6.2, 8.0, and 9.0 m) were 3.73 mg/L and 1.48 mg/L; across all epilimnetic depths (0.1, 1.6, and 3.8 m) they were 0.41 mg/L and 0.14 mg/L, respectively (Figures 4D-E). Substantial changes in epilimnetic concentrations were not observed until 24 hours prior to turnover.

Within that 24 hour period, average epilimnetic total Fe and total Mn increased by 70% (0.61 to 1.04 mg/L) and 66% (0.29 to 0.48 mg/L), respectively.

In contrast to the epilimnion, we observed declining total Fe and Mn concentrations in the hypolimnion prior to turnover (Figures 4D-E). Between 16 October and 02 November 2020, hypolimnetic total Fe and total Mn concentrations declined at a rate of 0.13 and 0.11 mg/L/d, respectively. However, there were also periods of fluctuations in total Fe and total Mn concentrations by as much as 1 mg/L/d (Figure 4D-E). In the 24 hours prior to turnover, average hypolimnetic total Fe and total Mn decreased by 45% (2.09 to 1.14 mg/L) and 32% (0.82 to 0.55 mg/L), respectively.

A strong concentration gradient between the epilimnion and hypolimnion remained for total Fe and total Mn until full reservoir turnover on 02 November 2020. After turnover, water temperature and DO rapidly equalized across the full water column, coinciding with the rapid equalization of total Fe and Mn concentrations across the water column (Figures 4D-E). Total Fe and Mn concentrations were lower and less variable than during the pre-turnover period (Figures 4D-E). The reservoir remained well-mixed for 2 days, but then shifting thermal gradients led to a temporary re-stratification that began on 02 November 2020 and lasted until the end of the deployment on 09 November 2020 (Figures 4A-B). The re-stratification of the reservoir was also evident in total Fe and total Mn concentrations (Figures 4D-E).

3.4 *Oxygen On Deployment*

3.4.1 *Water Temperature, Stratification, and DO*

DO concentrations, water temperature, and Schmidt stability differed considerably between the two deployments (Figures 5A-C). At the start of the Oxygen On deployment (26 May 2021), 16 days prior to HOx activation, epilimnetic DO concentrations were high (5-15 mg/L) and exhibited a consistent decline throughout the deployment due to warm air temperatures (Figure S14). Metalimnetic and hypolimnetic DO concentrations were both approximately 0 mg/L throughout the deployment. The water temperature profile shows distinctly stratified layers in the reservoir prior to HOx operation, with a sharp temperature gradient throughout the epilimnion for the entire deployment and a slight temperature gradient in the hypolimnion (Figure 5B). Immediately following HOx activation on 11 June 2021, the water temperature profile equalized across layers below 6m depth, indicating mixing within the hypolimnion due to HOx activation (Figure 5B). The water temperature profile in the epilimnion was unaffected by HOx operation. Metalimnetic and hypolimnetic DO concentrations did not increase above 0 mg/L in the few days after activation of the HOx system. This is attributed to chemical oxygen demand in the hypolimnion resulting from high concentrations of reduced solutes (e.g., Fe(II) and Mn(II)).

3.4.2 *Predicted Fe and Mn Concentrations*

At the beginning of the deployment, the highest concentrations of total Fe and

Mn were at the lowest depth (9m) and concentrations decreased upwards in the water column, with a sharp decrease between the hypolimnion and epilimnion (Figures 5D-E). In the first 24 hours of the deployment, total Fe and Mn concentrations averaged across all epilimnetic depths were 0.43 and 0.03 mg/L, respectively, while across the hypolimnetic depths they were 2.71 and 0.54 mg/L, respectively. Prior to HOx operation, both total Fe and Mn in the hypolimnion exhibited large, sub-daily fluctuations which resulted in concentration changes of up to 1.62 mg/L/hr and 0.19 mg/L/hr, respectively (Figures 5D-E). These sub-daily fluctuations were most pronounced at the lowest depth.

The spatial and temporal cycling dynamics of Fe and Mn were significantly affected by hypolimnetic oxygenation. Prior to activation of the HOx system on 11 June 2021, epilimnetic total Fe and Mn concentrations remained constant (sd = 0.07 mg/L and 0.004 mg/L, respectively) and low (maximum concentrations = 0.63 mg/L and 0.05 mg/L, respectively). Hypolimnetic total Fe and Mn concentrations during this period were much more variable (sd = 1.85 mg/L and 0.19 mg/L, respectively) and higher (maximum concentrations = 7.90 mg/L and 1.08 mg/L, respectively). Shortly after HOx activation, total Fe and Mn concentrations equalized contemporaneously with the equalization of water temperature across the hypolimnetic depths, indicating that this layer of the reservoir was well-mixed with respect to Fe and Mn (Figures 5B, 5D-E). In contrast, differences in total Fe and Mn concentrations across the epilimnetic depths increased slightly after activation of the HOx system.

Approximately 6 hours after turning on the HOx system, total Fe and Mn at 9m depth declined by approximately 2.5 mg/L and 0.25 mg/L, respectively (Figures 5D-E). Concentrations of total Fe and Mn at all hypolimnetic depths subsequently increased over the next 24 hours, before eventually stabilizing over the following 24 hours at concentrations of 1.5-3.5 mg/L and 0.5-0.75 mg/L, respectively. For the remainder of the deployment, total Fe and Mn concentrations remained equal across all hypolimnetic depths and exhibited less variability (Figures 5D-E).

3.5 *Predicted Fe and Mn Soluble-to-Total Ratios*

The ratio of predicted soluble to total Fe (SFe:TFe) and Mn (SMn:TMn) was calculated to assess redox transformations. We observed distinct changes in these ratios over the course of both deployments, most notably in the hypolimnion (Figure 6). During the Turnover Deployment, the hypolimnion was maintained at oxic conditions pre-turnover (due to HOx) and post-turnover (due to mixing). As expected, hypolimnetic SFe:TFe was approximately 0 during this entire deployment, indicating that all Fe in the hypolimnion was in the particulate fraction (soluble Fe + particulate Fe = total Fe). In contrast, hypolimnetic SMn:TMn was approximately 1 at the beginning of the deployment, indicating that all Mn was in the soluble fraction. However, in the week prior to turnover, hypolimnetic SMn:TMn oscillated between 0.5 and 1. Following turnover, SMn:TMn was greater than 0.75 and remained high until the end of the deployment.

At the beginning of the Oxygen On deployment, SFe:TFe differed greatly with depth in the hypolimnion, with ratios greater than 0.8 at 9m depth and ratios close to 0 at 6.2m and 8m depths (Figures 6C-D). Between the beginning of the deployment and HOx activation on 11 June 2021, the SFe:TFe at 6.2m and 8m increased continuously to approximately the same level as 9m (Figures 6C-D). Just before the initiation of HOx operation, the SFe:TFe at all hypolimnion depths was > 0.75, indicating that most of the Fe in the hypolimnion was in the soluble fraction. However, immediately after turning the HOx system on, the SFe:TFe in the hypolimnion decreased steadily. In the 48-hour period after HOx activation, the SFe:TFe in the hypolimnion declined to less than 0.25 and remained low until the end of the experimental period (Figure 6C-D), indicating oxidation processes. In contrast to Fe, SMn:TMn in the hypolimnion was $>$ 0.90 for the entire deployment. We did not observe a significant effect of HOx operation on SMn:TMn (0.99 pre-HOx, 0.97 post-HOx).

4. Discussion

4.1 *PLSR modeling of high frequency absorbance spectra can predict Fe and Mn concentrations*

Using UV-visible absorbance spectra and PLSR modeling, we made hourly predictions of Fe and Mn concentrations at 6 depths in our study reservoir. Our results indicate that this method can successfully predict Fe and Mn concentrations based on their covariability with UV-vis absorbance spectra, despite the paucity of clearly-defined absorbance peaks for these elements. PLSR models were able to explain a high proportion of the variability in the sampling data (Table 1) and predictions agreed with expected Fe and Mn cycling dynamics. For example, the rapid decline in SFe:TFe following the onset of HOx operation (Figure 6C) matches expectations based on the rapid oxidation kinetics of Fe(II) in the presence of oxygen (Davison & Seed 1983); previous studies have also demonstrated substantial decreases in soluble Fe following short periods of HOx (Dent et al. 2014, Munger et al. 2016, Krueger et al. 2020). Based on model skill metrics (i.e., R^2 and RMSEP) and visual inspection of the predicted time series, accurate predictions of Fe and Mn concentrations using this method are influenced by numerous factors, including: the range and variance of concentrations in the calibration dataset, the sample size used for calibration, the number of outliers in the calibration dataset, the number of components in the PLSR model, and the inherent predictability of each variable at a particular site (i.e., the strength of correlation with the UV-vis absorbance spectra).

Our results suggest that our methodology may be most appropriate for measuring elevated concentrations of Fe and Mn (> 0.1 mg/L). This result agrees with Vaughan et al. (2018), who suggested that the application of this method to predict riverine total phosphorus (TP) concentrations was best for sites with elevated TP (>0.1 mg/L) concentrations. In our study, PLSR models fit to data with lower concentrations of Fe and Mn (< 0.1 mg/L) generally did not perform well. For example, soluble Fe during the Turnover Deployment had median concentrations of 0.06 mg/L and 0.02 mg/L in the epilimnion and hypolimnion,

respectively (Figure 3 and Table S1). Accordingly, the PLSR models for soluble Fe had the lowest R^2 (epilimnion: 0.74; hypolimnion: 0.06) and highest RMSEP relative to median calibration concentration out of any model for the Turnover Deployment (Tables 1, S1).

Our PLSR models were also sensitive to the range and variance of sampling data used for calibration. Preliminary model testing revealed that PLSR models were hindered by the distinct water chemistry between epilimnetic and hypolimnetic depths (Fe and Mn mean differences >1.3 mg/L and 0.8 mg/L, respectively; see Figure 3) and therefore models were generated separately for each reservoir layer. This conforms with findings of previous studies using *in situ* UV-vis spectrophotometers and PLSR in waterbodies, which all achieved higher accuracy with site-specific models (Avagyan, Runkle, & Kutzbach 2014, Vaughan et al. 2018, Etheridge et al. 2014). However, when comparing pairs of PLSR models (i.e., the same variable + depth combination) between the two deployments, the models fit to data with a higher standard deviation had higher R^2 values, with the sole exception of hypolimnetic total Fe (Tables 1 and S1). These results suggest that there is a tradeoff between capturing the maximum variability in observed concentrations and the limitations imposed by the degree of covariability between the UV-vis absorbance spectra and the variable of interest (also observed by Avagyan, Runkle, & Kutzbach 2014 and Allen 2021). To achieve an accurate predictive model, grouping data based on the spatial and temporal context of measurement achieved a better fitting model while still maximizing the variability captured in the calibration data.

Birgand et al. (2016) used a similar approach for making predictions of soluble Fe concentrations in FCR after the activation of a HOx system. They obtained a slightly better model fit, indicated by an R^2 value of 0.94, compared to our R^2 values of 0.79 and 0.75 (epilimnion and hypolimnion, respectively) for the Oxygen On Deployment. We used calibration sample sizes of 48 and 45 (epilimnion and hypolimnion, respectively) while Birgand et al. (2016) used 27. However, they used 5 components in their PLSR model, whereas we used 4 components. Thus, the higher R^2 value for their model may be attributed to a higher ratio of components to sample size (18%) compared to our study (8-9%).

4.2 *Fe and Mn Concentrations Change Gradually in Response to Weakening Stratification and Rapidly in Response to Full Turnover*

Trends in predicted Fe and Mn concentrations shed light on the changes that occurred in the reservoir before and after turnover. Hypolimnetic concentrations of Fe and Mn began declining 17 and 9 days prior to turnover, respectively, and shorter periods of more rapid concentration fluctuations were superimposed upon these patterns of decline (Figures 4D-E). Combined, these results suggest that turnover, at least in our study reservoir, is not a discrete event, but rather a process occurring over an extended time period. McMahon (1969) measured a similar decrease in soluble Fe using daily samples for nine days across spring mixing in a dimictic lake; soluble Fe concentrations decreased by more than one order of magnitude 5 days prior to full circulation. McMahon (1969) did not

offer any interpretation of this phenomenon, simply stating that the changes in soluble Fe were concurrent with vernal circulation. Similar trends have also been observed in other parameters of biogeochemical relevance. For example, Kankaala et al. (2007) found that the majority of CH_4 in the hypolimnion of a lake was microbially oxidized at the oxycline boundary during a month-long period of weakening stratification before complete mixing occurred, resulting in lower effluxes of CH_4 to the atmosphere during turnover.

Predicted Fe and Mn concentration data can be compared to other time series data to infer mechanisms behind the declining Fe and Mn concentrations prior to turnover. Based on trends in Schmidt stability and water temperature (Figures 4A-B), reservoir stratification was weakening for a 9-day period prior to full turnover, in response to daily and hourly shifts in meteorological conditions, including air temperature and wind speed (Figure S13). Mixing between the hypolimnion and metalimnion, as indicated by the homogenization of water temperature between these layers, occurred periodically throughout the deployment, with an increasing frequency as turnover approached (Figures 4A-B, S15). These ephemeral periods of mixing between the hypolimnion and metalimnion likely led to exchange of Fe and Mn between layers, which suggests that hydrodynamic processes occurring on hourly to daily time scales may have a substantial influence of Fe and Mn cycling. However, without Fe and Mn concentration data at a high spatiotemporal resolution, these patterns would not be observed.

The flexibility of using a multiplexor-spectrophotometer system with a customized prediction algorithm (e.g., site-specific PLSR models) allows for the quantification of high-resolution elemental stoichiometry by making predictions of both the soluble and total fractions of Fe and Mn. During the Turnover Deployment, Fe was predominantly composed of the total fraction, whereas Mn was largely composed of the soluble fraction until approximately one week before turnover, at which time the SMn:TMn ratio began to decline (Figure 6B). This coincided with the onset of declining total Mn concentrations that continued until turnover, excluding a 2-day period from 28 October to 30 October 2020 when total Mn concentrations temporarily increased (Figure 4E). The shift to declining SMn:TMn and total Mn concentrations also coincided with increased frequency of mixing between the metalimnion and hypolimnion and declining stratification intensity (Figures 4A-B and 6B). These trends suggest that declining total Mn concentrations in the pre-turnover period were the result of increased oxidation of Mn(II), perhaps due to the exposure of Mn(II) in the hypolimnion to Mn-oxidizing microbes that inhabit the metalimnion, as demonstrated by a previous study at FCR showing that the presence of Mn-oxidizing microorganisms can substantially increase Mn oxidation rates (Munger et al. 2016).

4.3 *Hypolimnetic Oxygenation Causes Oxidation of Fe, but not Mn*

The MUX-spectrophotometer system enabled us to observe Fe and Mn concentration changes in response to hypolimnetic oxygenation at an unprecedented

spatiotemporal resolution. Fe and Mn concentrations in the hypolimnion both spiked in the 48 hours following oxygenation, then declined (Figures 5D-E). However, Fe concentrations decreased to levels lower than they were prior to oxygenation, especially at the lowest depth, whereas Mn concentrations declined to approximately the same levels prior to oxygenation (Figures 5D-E). These results indicate that the HOx system effectively physically mixed the hypolimnion with respect to both metals, as total Fe and total Mn concentrations quickly converged across hypolimnetic depths after turning on the HOx system (Figures 5D-E) The physical mixing induced by the HOx system appeared to affect Fe and Mn similarly, suggesting that the spike in total Fe and Mn immediately following HOx activation was a result of increased mixing and/or entrainment of particulates in the hypolimnion due to stirring of the bottom sediments. The convergence of Fe and Mn concentrations across hypolimnetic depths has previously been observed in response to HOx activation (Gerling et al. 2014), but results from this study reveal that this can occur in less than 24 hours, and may subsequently be followed by an ephemeral spike in total Fe and Mn concentrations.

Concentrations of total Fe and Mn displayed much greater short-term variability prior to HOx activation than they did post-activation. This was especially pronounced at the lowest depth (9 m) where concentrations fluctuated significantly over a period of less than 24 hours (Figures 5D-E). Given that the SFe:TFe ratio in the upper and middle hypolimnion (6.2m and 8m) steadily increased during the pre-HOx period (Figure 6C), likely due to diffusion of soluble Fe out of the lower hypolimnion, the rapid fluctuations in total Fe in the lower hypolimnion may have been attributed to shifting diffusion gradients. However, similar patterns in short-term variability were observed in Fe and Mn, despite the fact that Mn was predominantly in the soluble phase for the entire deployment, suggesting that diffusion of soluble Mn out of the lower hypolimnion was not responsible for the pre-HOx rapid fluctuations observed at 9 m.

The change in redox conditions caused by adding DO to the hypolimnion had a much more pronounced effect on Fe than Mn, as has been observed in other studies (e.g., Gantzer et al. 2009). The contrasting responses of Fe and Mn to oxygenation can be seen most clearly in the resulting changes in soluble:total ratios (Figure 6). The SFe:TFe ratio in the hypolimnion exhibited a nearly constant linear decline in the 48 hours post-oxygenation and remained below 0.25 for the remainder of the deployment. This indicates that soluble Fe in the water column was rapidly oxidized by the HOx system, even though there was no measurable increase in hypolimnetic DO. This is further supported by the fact that the mean hypolimnetic total Fe concentration was consistently lower after HOx operation began than it was previously. The observed trends in SFe:TFe ratios agree with previous research on the effects of HOx systems on Fe in lakes and reservoirs. For example, Dent et al. (2014) found that SFe:TFe declined to 0.58 after 8 hours of hypolimnetic oxygenation. In our study, it took approximately twice as long (16 hours) for SFe:TFe to reach 0.58. However, the Fe concentrations in Dent et al. (2014) were lower (0.17 - 2.88 mg/L) than those

in our study (0.31 - 7.42 mg/L).

In contrast to Fe, the SMn:TMn ratio in the hypolimnion displayed only a very slight response (approximately 2% decrease) to HOx activation, demonstrating that hypolimnetic oxygenation did not result in significant oxidation of Mn. Our results agree with those from Dent et al. (2014), who found that Mn was still 100% in the soluble phase 8 hours after oxygenation. Furthermore, previous studies at FCR have also showed that soluble Mn does not respond significantly to oxygenation alone and that other factors, such as microbially-mediated oxidation, reservoir pH (range 6.4 - 7.1 observed in the hypolimnion during our study) and dilution from physical mixing, are more important variables impacting hypolimnetic soluble Mn than oxygenation (Munger et al. 2016, Krueger et al. 2020).

4.4 *Study Limitations*

The MUX pumping system enabled us to monitor multiple depths simultaneously, which is invaluable for investigating biogeochemical processes in spatially heterogeneous systems such as thermally-stratified reservoirs. However, there are several limitations to be improved upon in future research. In our reservoir, the cuvette fitted on the spectrophotometer experienced fouling, likely due to Fe and Mn in the hypolimnion that oxidized and precipitated on the cuvette walls upon exposure to oxygen. Despite our efforts to limit fouling (see Methods), there was still a fouling signal detected in several periods of our time series (Figures S4-5). PLSR models provided a remarkably good numerical correction for this fouling signal, indicating that the collection of additional calibration samples obtained at regular intervals between servicing dates may yield lower uncertainties in future deployments. We also found that truncating the UV-vis absorbance spectra used for calibration to only include wavelengths greater than 250 nm substantially improved the model skill and diminished spikes in the time series of predictions that corresponded to periods of heavy fouling (Figures S6-7).

Our results captured sub-weekly patterns in Fe and Mn dynamics in FCR, but the PLSR-predicted time series of Fe and Mn concentrations was not able to adequately capture some of the high-magnitude, sub-daily fluctuations that were observed in the sampling data (Figures 4 and 6). This is likely due to varying PLSR model skill, which is related to the sample size and distribution of data used for calibration, the number of PLSR model components, and the inherent predictability of each variable. Therefore, it follows that the strength of correlation between the UV-vis absorbance spectra and Fe/Mn concentrations plays a strong role in determining the limits to the temporal resolution. This relationship can be refined through the methodological suggestions outlined above, but ultimately depends upon the spectral properties of the study system.

5. Conclusions

Results from this study demonstrate that coupling a spectrophotometer with a pumping system enabled unprecedented high-frequency monitoring of Fe and

Mn at multiple depths in our study reservoir, providing a unique ability to observe hour-resolution biogeochemical dynamics in a freshwater ecosystem. Our findings underscore the importance of implementing robust and consistent methodologies for obtaining calibration concentrations, choosing the number of components in PLSR models, and quantifying the uncertainty around predictions.

The high-spatio-temporal resolution predictions provide novel insights into Fe and Mn cycling dynamics that could improve aquatic monitoring programs and reservoir management practices. First, we demonstrated that Fe and Mn concentrations can fluctuate significantly on time scales much shorter than those employed by most traditional monitoring programs. For example, sub-daily fluctuations of total Fe and Mn during the Oxygen On Deployment resulted in concentration changes of up to 1.62 mg/L/hr and 0.19 mg/L/hr, respectively. Considering that the secondary drinking water standards for Fe and Mn are 0.3 and 0.05 mg/L, respectively, sub-daily concentration changes of this magnitude are critical for water quality management. Second, we observed an increase in total hypolimnetic Fe and Mn in response to the re-stratification of our study reservoir two days after turnover, which contradicts the common assumption that metals concentrations equalize and remain consistently low during the mixed period following turnover. Last, our results offer new insights on the rapid response of Fe to hypolimnetic oxygenation; within hours of activating the system, the soluble to total Fe ratio indicated oxidation of Fe, even though there was no measurable increase in DO. This study emphasizes the power of high spatiotemporal resolution data for improving our understanding of biogeochemical cycles by unveiling previously-unobserved processes altering Fe and Mn cycling.

Data Availability

All observational data, including the spectrophotometer data, are published in the Environmental Data Initiative repository (Carey et al. 2022a, Carey et al. 2022b, Carey et al. 2022c, Schreiber et al. 2022, Hammond et al. 2022). All code used to analyze the spectrophotometer data with PLSR and generate the figures is available in the Zenodo repository (Hammond 2022).

Declaration of competing interest

The authors declare that they have no known competing financial interests or personal relationships that could have appeared to influence the work reported in this paper.

Acknowledgements

This work has been supported by the Virginia Tech Cunningham Doctoral Fellowship, the Geological Society of America Graduate Research Grant Program, and the National Science Foundation (DEB-1753639, CNS-1737424, DBI-1933016). We gratefully acknowledge the Western Virginia Water Authority for allowing us access to the reservoir to conduct these experiments and Jeff Parks

for ICP-MS analysis. We also thank Abby Lewis, Heather Wander, and the entire Virginia Tech Reservoir Group research team for field support.

References

Allen, E. L. Water Quality Signatures of Switchgrass (*Panicum Virgatum*) Intercropped in Managed Forests and Mixed Land Use in the Southeastern United States. *ProQuest Dissertations and Theses* (North Carolina State University PP - United States -- North Carolina, 2021).

Avagyan, A., Runkle, B.R.K., Kutzbach, L., 2014. Application of high-resolution spectral absorbance measurements to determine dissolved organic carbon concentration in remote areas. J. Hydrol. 517, 435–446. https://doi.org/10.1016/j.jhydrol.2014.05.060

Beutel, M.W., Horne, A.J., 1999. A review of the effects of hypolimnetic oxygenation on lake and reservoir water quality. Lake Reserv. Manag. 15, 285–297. https://doi.org/10.1080/07438149909354124

Beutel, M.W., Leonard, T.M., Dent, S.R., Moore, B.C., 2008. Effects of aerobic and anaerobic conditions on P, N, Fe, Mn, and Hg accumulation in waters overlaying profundal sediments of an oligo-mesotrophic lake. Water Res. 42, 1953–1962. https://doi.org/10.1016/j.watres.2007.11.027

Bieroza, M.Z., Heathwaite, A.L., 2016. Unravelling organic matter and nutrient biogeochemistry in groundwater-fed rivers under baseflow conditions: Uncertainty in in situ high-frequency analysis. Sci. Total Environ. 572, 1520–1533. https://doi.org/10.1016/j.scitotenv.2016.02.046

Birgand, F., Aveni-Deforge, K., Smith, B., Maxwell, B., Horstman, M., Gerling, A.B., Carey, C.C., 2016. First report of a novel multiplexer pumping system coupled to a water quality probe to collect high temporal frequency in situ water chemistry measurements at multiple sites. Limnol. Oceanogr. Methods 14, 767–783. https://doi.org/10.1002/lom3.10122

Bryant, L.D., Hsu-Kim, H., Gantzer, P.A., Little, J.C., 2011. Solving the problem at the source: Controlling Mn release at the sediment-water interface via hypolimnetic oxygenation. Water Res. 45, 6381–6392. https://doi.org/10.1016/j.watres.2011.09.030

[dataset] Carey, C.C., A. Breef-Pilz, and B.J. Bookout. 2022a. Time series of high-frequency meteorological data at Falling Creek Reservoir, Virginia, USA 2015-2021 ver 6. Environmental Data Initiative. https://doi.org/10.6073/pasta/35d8d3f9390408f12d39e44e3f03abbe (Accessed 2022-09-30).

[dataset] Carey, C.C., A. Breef-Pilz, W.M. Woelmer, and B.J. Bookout. 2022b. Time series of high-frequency sensor data measuring water temperature, dissolved oxygen, pressure, conductivity, specific conductance, total dissolved solids, chlorophyll a, phycocyanin, and fluorescent

dissolved organic matter at discrete depths in Falling Creek Reservoir, Virginia, USA in 2018-2021 ver 6. Environmental Data Initiative. https://doi.org/10.6073/pasta/81c6c76f4fe22434a20aa8c00f2d4ad1 (Accessed 2022-02-02).

[dataset] Carey, C.C., A.S. Lewis, D.W. Howard, W.M. Woelmer, P.A. Gantzer, K.A. Bierlein, J.C. Little, and WVWA. 2022c. Bathymetry and watershed area for Falling Creek Reservoir, Beaverdam Reservoir, and Carvins Cove Reservoir ver 1. Environmental Data Initiative. https://doi.org/10.6073/pasta/352735344150f7e77d2bc18b69a22412 (Accessed 2022-11-16).

Carey, C.C., Woelmer, W.M., Lofton, M.E., Figueiredo, R.J., Bookout, B.J., Corrigan, R.S., Daneshmand, V., Hounshell, A.G., Howard, D.W., Lewis, A.S.L., McClure, R.P., Wander, H.L., Ward, N.K., Thomas, R.Q., 2022. Advancing lake and reservoir water quality management with near-term, iterative ecological forecasting. Inl. Waters 12, 107–120. https://doi.org/10.1080/20442041.2020.1816421

Cao, D.S., Deng, Z.K., Zhu, M.F., Yao, Z.J., Dong, J., Zhao, R.G., 2017. Ensemble partial least squares regression for descriptor selection, outlier detection, applicability domain assessment, and ensemble modeling in QSAR/QSPR modeling. J. Chemom. 31, 1–17. https://doi.org/10.1002/cem.2922

Chapman, M.J., Cravotta, C.A., Szabo, Z., Lindsey, B.D., 2013. Naturally Occurring Contaminants in the Piedmont and Blue Ridge Crystalline-rock Aquifers and Piedmont Early Mesozoic Basin Siliciclastic-rock Aquifers, Eastern United States, 1994-2008. US Department of the Interior, US Geological Survey.

Coraggio, E., Han, D., Gronow, C., Tryfonas, T., 2022. Water Quality Sampling Frequency Analysis of Surface Freshwater: A Case Study on Bristol Floating Harbour. Front. Sustain. Cities 3, 1–14. https://doi.org/10.3389/frsc.2021.791595

Davison, W., Seed, G., 1983. The kinetics of the oxidation of ferrous iron in synthetic and natural waters. Geochim. Cosmochim. Acta 47, 67–79. https://doi.org/10.1016/0016-7037(83)90091-1

Davison, W., 1993. Iron and manganese in lakes. Earth Sci. Rev. 34, 119–163. https://doi.org/10.1016/0012-8252(93)90029-7

Denham, M.C., 1997. Prediction intervals in partial least squares. J. Chemom. 11, 39–52. https://doi.org/10.1002/(SICI)1099-128X(199701)11:1<39::AID-CEM433>3.0.CO;2-S

Dent, S.R., Beutel, M.W., Gantzer, P., Moore, B.C., 2014. Response of methylmercury, total mercury, iron and manganese to oxygenation of an anoxic hypolimnion in North Twin lake, Washington. Lake Reserv. Manag. 30, 119–130. https://doi.org/10.1080/10402381.2014.898350

Difoggio, R., 2000. Guidelines for applying chemometrics to spectra: Feasibility and error propagation. Appl. Spectrosc. 54. https://doi.org/10.1366/0003702001949546

Etheridge, J.R., Birgand, F., Osborne, J.A., Osburn, C.L., Burchell, M.R., Irving, J., 2014. Using in situ ultraviolet-visual spectroscopy to measure nitrogen, carbon, phosphorus, and suspended solids concentrations at a high frequency in a brackish tidal marsh. Limnol. Oceanogr. Methods 12, 10–22. https://doi.org/10.4319/lom.2014.12.10

Gantzer, P.A., Bryant, L.D., Little, J.C., 2009. Controlling soluble iron and manganese in a water-supply reservoir using hypolimnetic oxygenation. Water Res. 43, 1285–1294. https://doi.org/10.1016/j.watres.2008.12.019

Gerling, A.B., Browne, R.G., Gantzer, P.A., Mobley, M.H., Little, J.C., Carey, C.C., 2014. First report of the successful operation of a side stream supersaturation hypolimnetic oxygenation system in a eutrophic, shallow reservoir. Water Res. 67, 129–143. https://doi.org/10.1016/j.watres.2014.09.002

[dataset] Hammond, N.W., F. Birgand, C.C. Carey, A. Breef-Pilz, B. Bookout, and M.E. Schreiber. 2022. Time series of in situ ultraviolet-visible absorbance spectra and high-frequency predictions of total and soluble Fe and Mn concentrations measured at multiple depths in Falling Creek Reservoir (Vinton, VA, USA) in 2020 and 2021 ver 4. Environmental Data Initiative. Retrieved from https://portal-s.edirepository.org/nis/mapbrowse?packageid=edi.974.4.

Hammond, N.W. 2022. High-frequency sensor data capture short-term variability in Fe and Mn cycling due to hypolimnetic oxygenation and seasonal dynamics in a drinking water reservoir. https://doi.org/10.5281/zenodo.7339718

Hem, J.D., 1972. Chemical Factors that Influence the Availability of Iron and Manganese in Aqueous Systems. Geol. Soc. Am. Bull. 83, 443–450.

Idso, S.B., 1973. On the concept of Lake Stability. Limnol. Oceanogr. 18, 681–683.

Istvánovics, V., Osztoics, A., Honti, M., 2004. Dynamics and ecological significance of daily internal load of phosphorus in shallow Lake Balaton, Hungary. Freshw. Biol. 49, 232–252. https://doi.org/10.1111/j.1365-2427.2004.01180.x

Kankaala, P., Taipale, S., Nykänen, H., Jones, R.I., 2007. Oxidation, efflux, and isotopic fractionation of methane during autumnal turnover in a polyhumic, boreal lake. J. Geophys. Res. Biogeosciences 112, 1–7. https://doi.org/10.1029/2006JG000336

Kritzberg, E.S., Hasselquist, E.M., Škerlep, M., Löfgren, S., Olsson, O., Stadmark, J., Valinia, S., Hansson, L.A., Laudon, H., 2020. Browning of freshwaters: Consequences to ecosystem services, underlying drivers, and potential mitigation measures. Ambio 49, 375–390. https://doi.org/10.1007/s13280-019-01227-5

Krueger, K.M., Vavrus, C.E., Lofton, M.E., McClure, R.P., Gantzer, P., Carey, C.C., Schreiber, M.E., 2020. Iron and manganese fluxes across the sediment-water interface in a drinking water reservoir. Water Res. 182, 116003. https://doi.org/10.1016/j.watres.2020.116003

Kruse, P., 2018. Review on water quality sensors. J. Phys. D. Appl. Phys. 51. https://doi.org/10.1088/1361-6463/aabb93

Kurz, M.J., de Montety, V., Martin, J.B., Cohen, M.J., Foster, C.R., 2013. Controls on diel metal cycles in a biologically productive carbonate-dominated river. Chem. Geol. 358, 61–74. https://doi.org/10.1016/j.chemgeo.2013.08.042

Marcé, R., George, G., Buscarinu, P., Deidda, M., Dunalska, J., De Eyto, E., Flaim, G., Grossart, H.P., Istvanovics, V., Lenhardt, M., Moreno-Ostos, E., Obrador, B., Ostrovsky, I., Pierson, D.C., Potužák, J., Poikane, S., Rinke, K., Rodríguez-Mozaz, S., Staehr, P.A., Šumberová, K., Waajen, G., Weyhenmeyer, G.A., Weathers, K.C., Zion, M., Ibelings, B.W., Jennings, E., 2016. Automatic High Frequency Monitoring for Improved Lake and Reservoir Management. Environ. Sci. Technol. 50, 10780–10794. https://doi.org/10.1021/acs.est.6b01604

McClain, M.E., Boyer, E.W., Dent, C.L., Gergel, S.E., Grimm, N.B., Groffman, P.M., Hart, S.C., Harvey, J.W., Johnston, C.A., Mayorga, E., McDowell, W.H., Pinay, G., 2003. Biogeochemical Hot Spots and Hot Moments at the Interface of Terrestrial and Aquatic Ecosystems. Ecosystems 6, 301–312. https://doi.org/10.1007/s10021-003-0161-9

McClure, R.P., Hamre, K.D., Niederlehner, B.R., Munger, Z.W., Chen, S., Lofton, M.E., Schreiber, M.E., Carey, C.C., 2018. Metalimnetic oxygen minima alter the vertical profiles of carbon dioxide and methane in a managed freshwater reservoir. Sci. Total Environ. 636, 610–620. https://doi.org/10.1016/j.scitotenv.2018.04.255

McMahon, J.W., 1969. the Annual and Diurnal Variation in the Vertical Distribution of Acid-Soluble Ferrous and Total Iron in a Small Dimictic Lake. Limnol. Oceanogr. 14, 357–367. https://doi.org/10.4319/lo.1969.14.3.0357

Mevik, B.H., Wehrens, R., and Liland, K.H. (2020). pls: Partial Least Squares and Principal Component Regression. R package version 2.7-3. https://CRAN.R-project.org/package=pls

Munger, Z.W., Carey, C.C., Gerling, A.B., Hamre, K.D., Doubek, J.P., Klepatzki, S.D., McClure, R.P., Schreiber, M.E., 2016. Effectiveness of hypolimnetic oxygenation for preventing accumulation of Fe and Mn in a drinking water reservoir. Water Res. 106, 1–14. https://doi.org/10.1016/j.watres.2016.09.038

Munger, Z.W., Carey, C.C., Gerling, A.B., Doubek, J.P., Hamre, K.D., McClure, R.P., Schreiber, M.E., 2019. Oxygenation and hydrologic controls on iron and manganese mass budgets in a drinking-water reservoir. Lake Reserv. Manag. 35, 277–291. https://doi.org/10.1080/10402381.2018.1545811

Nimick, D.A., Gammons, C.H., Parker, S.R., 2011. Diel biogeochemical processes and their effect on the aqueous chemistry of streams: A review. Chem. Geol. 283, 3–17. https://doi.org/10.1016/j.chemgeo.2010.08.017

Porter, J.H., Nagy, E., Kratz, T.K., Hanson, P., Collins, S.L., Arzberger, P., 2009. New eyes on the world: Advanced sensors for ecology. Bioscience 59,

385–397. https://doi.org/10.1525/bio.2009.59.5.6

Poulin, B.A., Ryan, J.N., Aiken, G.R., 2014. Effects of iron on optical properties of dissolved organic matter. Environ. Sci. Technol. 48, 10098–10106. https://doi.org/10.1021/es502670r

Preece, E.P., Moore, B.C., Skinner, M.M., Child, A., Dent, S., 2019. A review of the biological and chemical effects of hypolimnetic oxygenation. Lake Reserv. Manag. 35, 229–246. https://doi.org/10.1080/10402381.2019.1580325

R Core Team (2022). R: A language and environment for statistical computing. R Foundation for Statistical Computing, Vienna, Austria. URL https://www.R-project.org/.

Rieger, L., Langergraber, G., Siegrist, H., 2006. Uncertainties of spectral in situ measurements in wastewater using different calibration approaches. Water Sci. Technol. 53, 187–197. https://doi.org/10.2166/wst.2006.421

Rode, M., Wade, A.J., Cohen, M.J., Hensley, R.T., Bowes, M.J., Kirchner, J.W., Arhonditsis, G.B., Jordan, P., Kronvang, B., Halliday, S.J., Skeffington, R.A., Rozemeijer, J.C., Aubert, A.H., Rinke, K., Jomaa, S., 2016. Sensors in the Stream: The High-Frequency Wave of the Present. Environ. Sci. Technol. 50, 10297–10307. https://doi.org/10.1021/acs.est.6b02155

Sakamoto, C.M., Johnson, K.S., Coletti, L.J., 2009. Improved algorithm for the computation of nitrate concentrations in seawater using an in situ ultraviolet spectrophotometer. Limnol. Oceanogr. Methods 7, 132–143. https://doi.org/10.1002/lom3.10209

[dataset] Schreiber, M.E., N.W. Hammond, K.M. Krueger, Z.W. Munger, C.L. Ming, A. Breef-Pilz, and C.C. Carey. 2022. Time series of total and soluble iron and manganese concentrations from Falling Creek Reservoir and Beaverdam Reservoir in southwestern Virginia, USA from 2014 through 2021 ver 6. Environmental Data Initiative. https://doi.org/10.6073/pasta/7cdf3d7a234963b265f09b7d6d08f357.

EPA. 2021. Secondary Drinking Water Standards: Guidance for Nuisance Chemicals. Available at: https://www.epa.gov/sdwa/secondary-drinking-water-standards-guidance-nuisance-chemicals. (Accessed: 22nd February 2021)

Vaughan, M.C.H., Bowden, W.B., Shanley, J.B., Vermilyea, A., Wemple, B., Schroth, A.W., 2018. Using in situ UV-Visible spectrophotometer sensors to quantify riverine phosphorus partitioning and concentration at a high frequency. Limnol. Oceanogr. Methods 16, 840–855. https://doi.org/10.1002/lom3.10287

Wasserman, G.A., Liu, X., Parvez, F., Ahsan, H., Levy, D., Factor-Litvak, P., Kline, J., van Geen, A., Slavkovich, V., Lolacono, N.J., Cheng, Z., Zheng, Y., Graziano, J.H., 2006. Water manganese exposure and children's intellectual function in Araihazar, Bangladesh. Environ. Health Perspect. 114, 124–129. https://doi.org/10.1289/ehp.8030

Weishaar, J.L., Aiken, G.R., Bergamaschi, B.A., Fram, M.S., Fujii, R., Mopper,

K., 2003. Evaluation of specific ultraviolet absorbance as an indicator of the chemical composition and reactivity of dissolved organic carbon. Environ. Sci. Technol. 37, 4702–4708. https://doi.org/10.1021/es030360x

Winslow, L., Read, J., Woolway, R., Brentrup, J., Leach, T., Zwart, J., Albers, S., Collinge, D., 2019. rLakeAnalyzer: Lake Physics Tools. R package version 1.11.4.1. https://CRAN.R-project.org/package=rLakeAnalyzer

Wold, S., Sjöström, M., Eriksson, L., 2001. PLS-regression: A basic tool of chemometrics. Chemom. Intell. Lab. Syst. 58, 109–130. https://doi.org/10.1016/S0169-7439(01)00155-1

Woodward, H.P., 1932. Geology and Mineral Resources of the Roanoke Area, Virginia, &c.

World Health Organization, 2017. Guidelines for Drinking - water Quality. Fourth Edition Incorporating the First Addendum. 10 Acceptability aspects : Taste , odour and appearance.

Xiao, N., Cao, D.S., Li, M.Z., and Xu, Q.S. (2019). enpls: Ensemble Partial Least Squares Regression. R package version 6.1. https://CRAN.R-project.org/package=enpls

Xiao, Y.H., Sara-Aho, T., Hartikainen, H., Vähätalo, A. V., 2013. Contribution of ferric iron to light absorption by chromophoric dissolved organic matter. Limnol. Oceanogr. 58, 653–662. https://doi.org/10.4319/lo.2013.58.2.0653

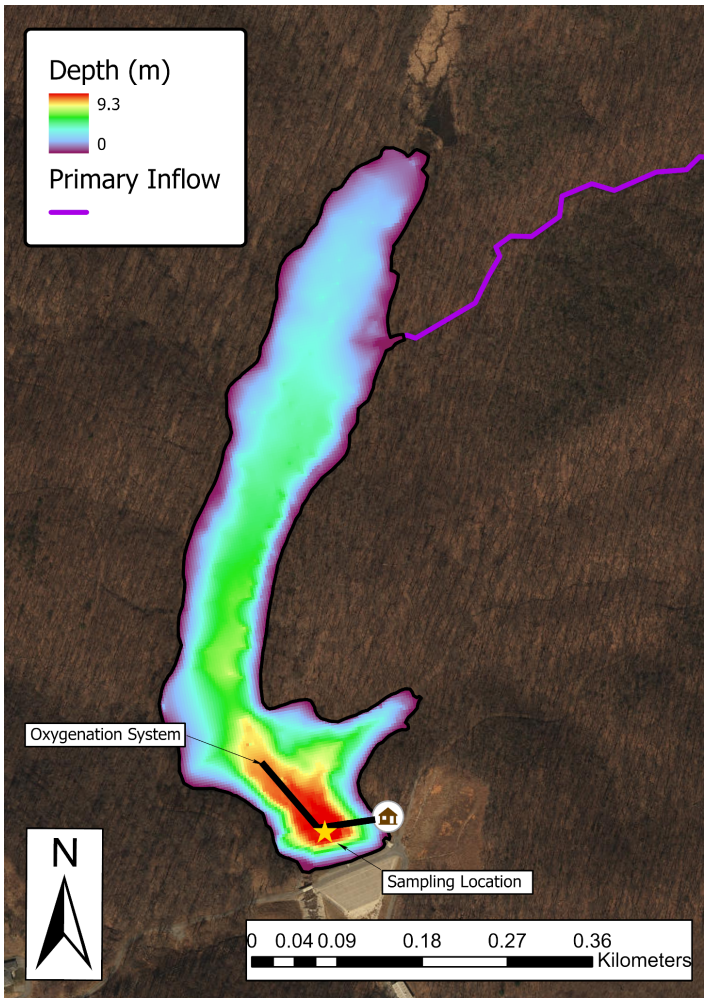

Figure 1. Bathymetric map of Falling Creek Reservoir, Vinton, VA, USA (37.302913°N, -79.837070°W) depicting the primary sampling location (star icon) and hypolimnetic oxygenation (HOx) system. The HOx system consists of outlet piping with a distribution header (black line) and an oxygen contact chamber (shed icon).

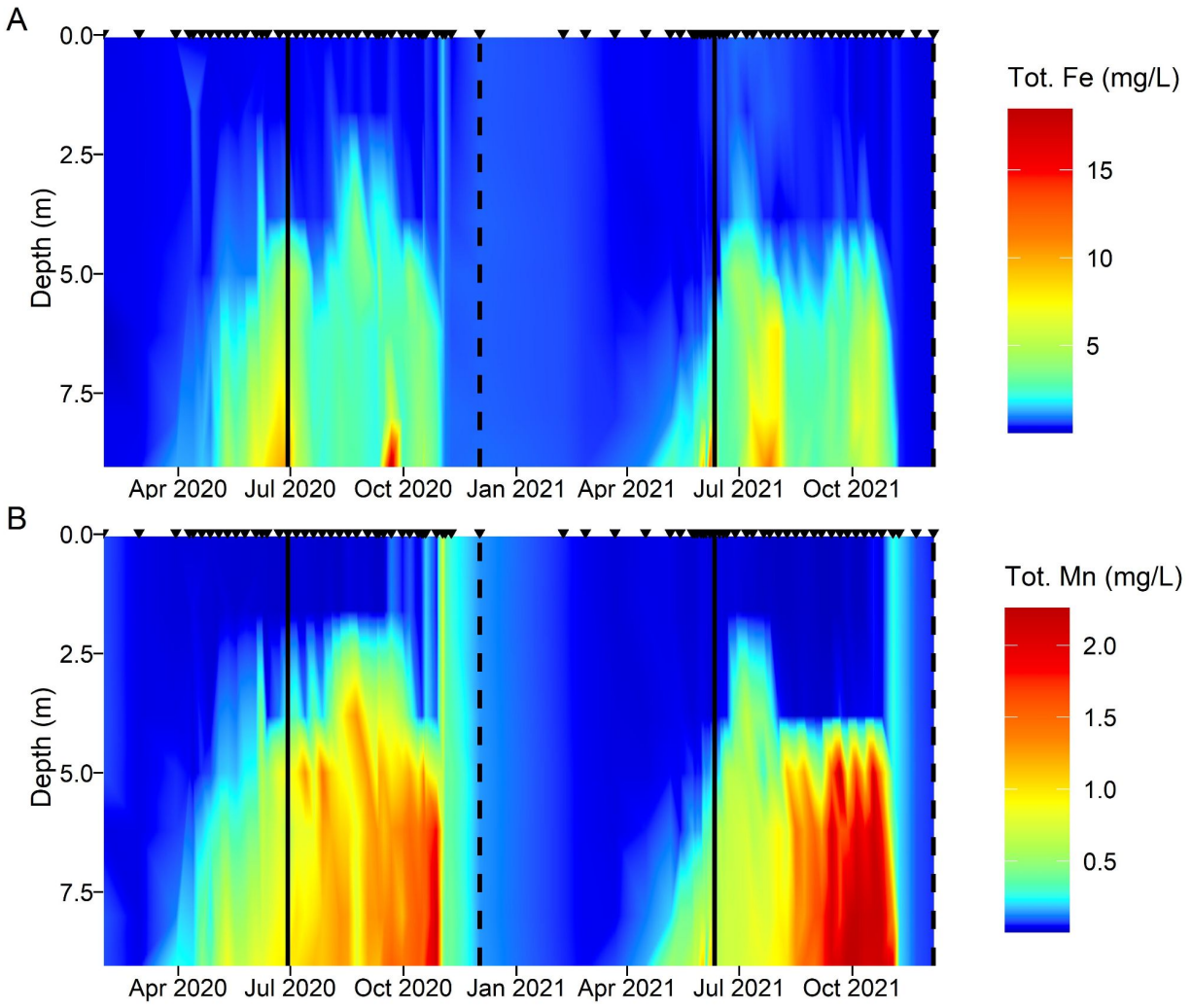

Figure 2. A) total Fe and B) total Mn concentrations in FCR from 2020 until 2021. Total Fe and Mn concentrations are derived from manual samples that are collected approximately weekly during the summer stratified period each year. The HOx system was activated on 29 June 2020 and 11 June 2021 (solid black vertical lines) and deactivated on 02 December 2020 and 06 December 2021 (dashed black vertical lines). Values are linearly interpolated for plotting purposes. Inverted triangles at the top of the panel indicate sampling times.

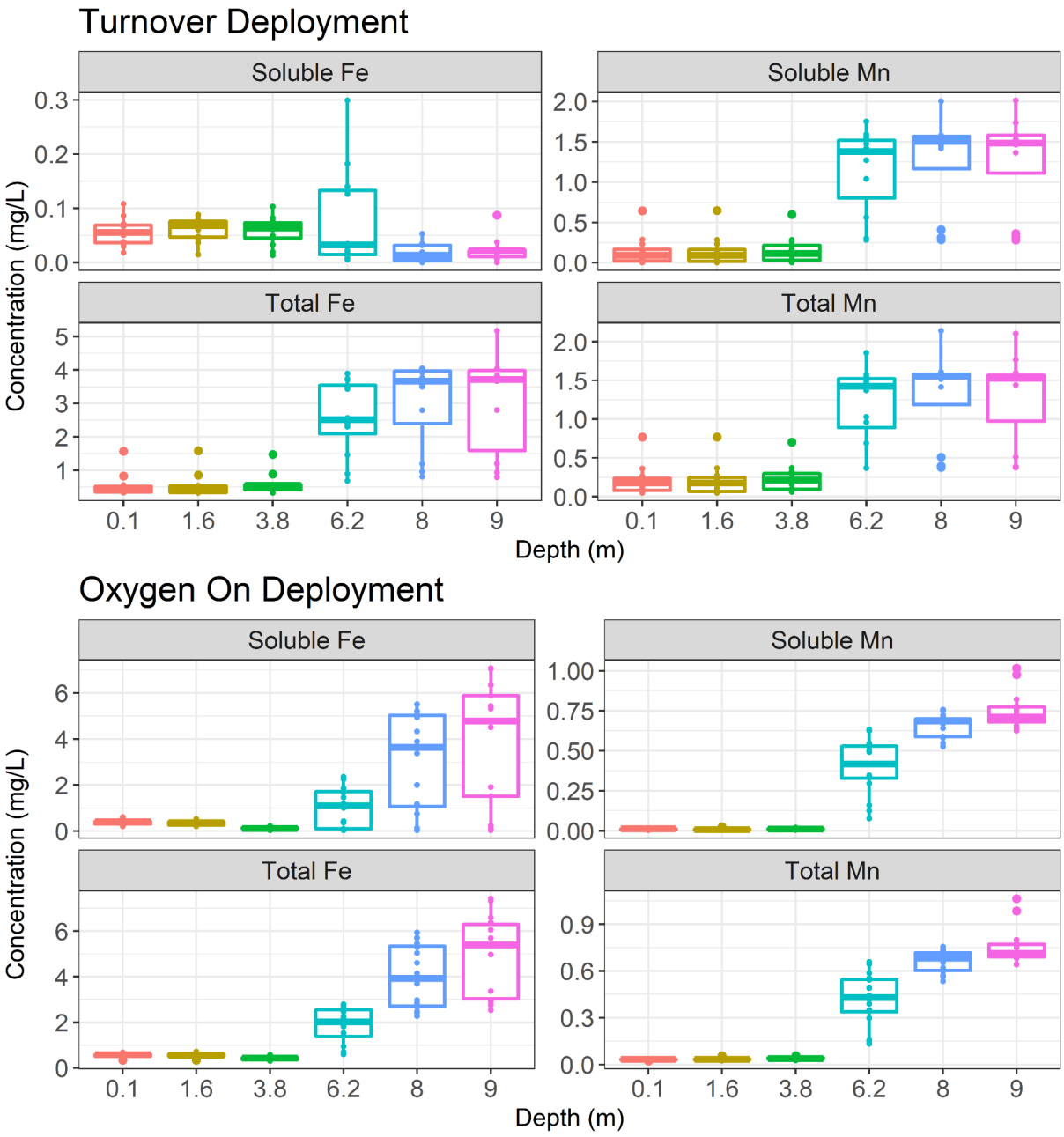

Figure 3: Sampling data used to calibrate PLSR models for the Reservoir Turnover Deployment (n = 69 for total and soluble Fe, 71 for total Mn, and 70 for soluble Mn) and the Oxygen On Deployment (n = 93 for all variables). Outliers (determined by the Monte Carlo predictive error distribution) are not

included. Note that the y-axes vary among panels.

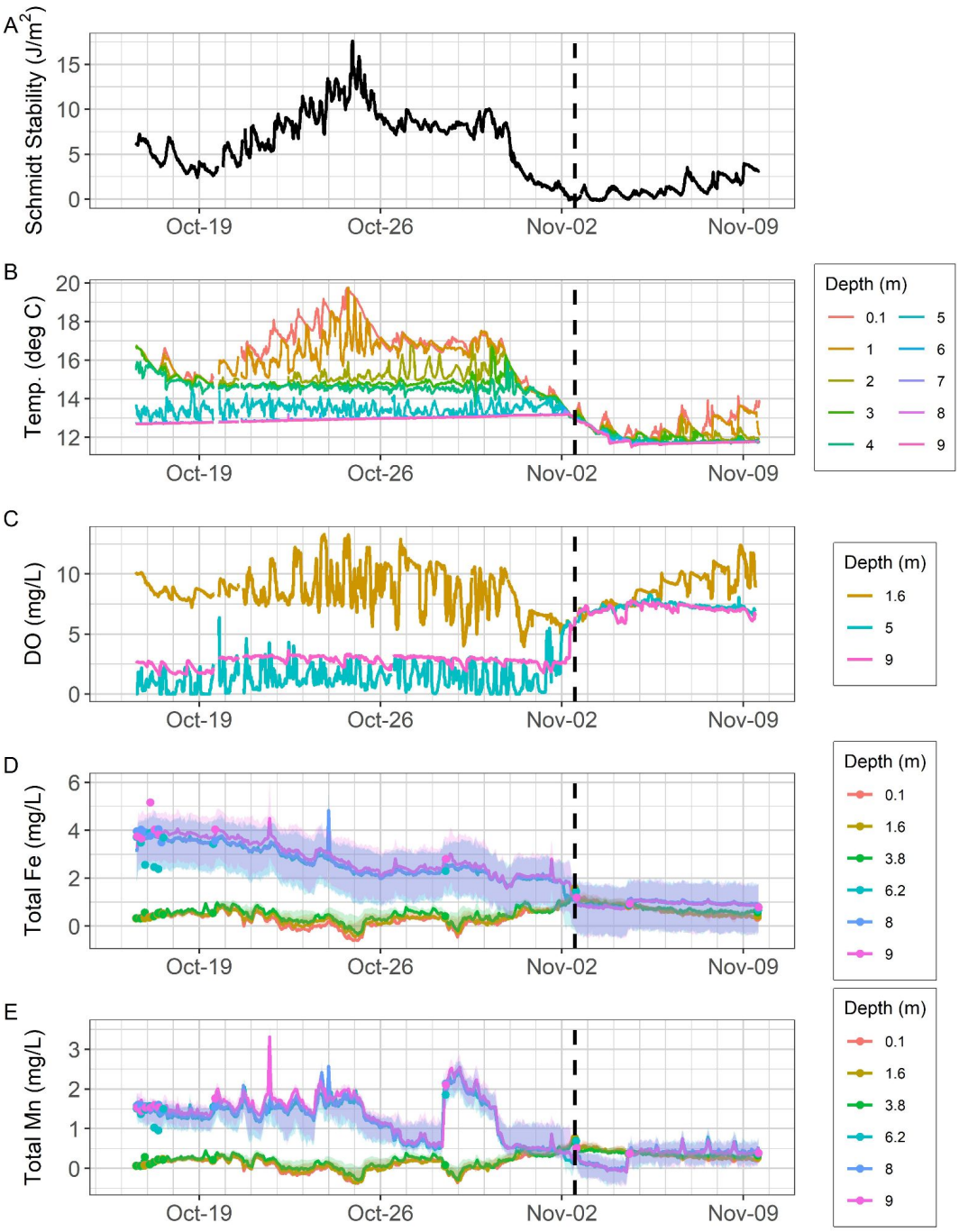

Figure 4. Time series plots of A) Schmidt stability, B) water temperature, C) dissolved oxygen, D) predicted total Fe concentrations (lines) with observed values (dots) and 90% predictive intervals (shaded areas), and E) predicted total Mn concentrations (lines) with observed values (dots) and 90% predictive intervals (shaded areas) during the Reservoir Turnover Deployment. The dashed vertical line on 02 November 2020 represents reservoir turnover, defined by the first time point at which the temperature differential between 0.1m and 9m was less than 1 degree Celsius. Colors of lines (PLSR predictions) and dots (samples) are shown on the color scale to the right. Note that the reservoir temporarily re-stratified after 02 November 2020. Time series plots for soluble Fe and Mn are shown in Figure S16.

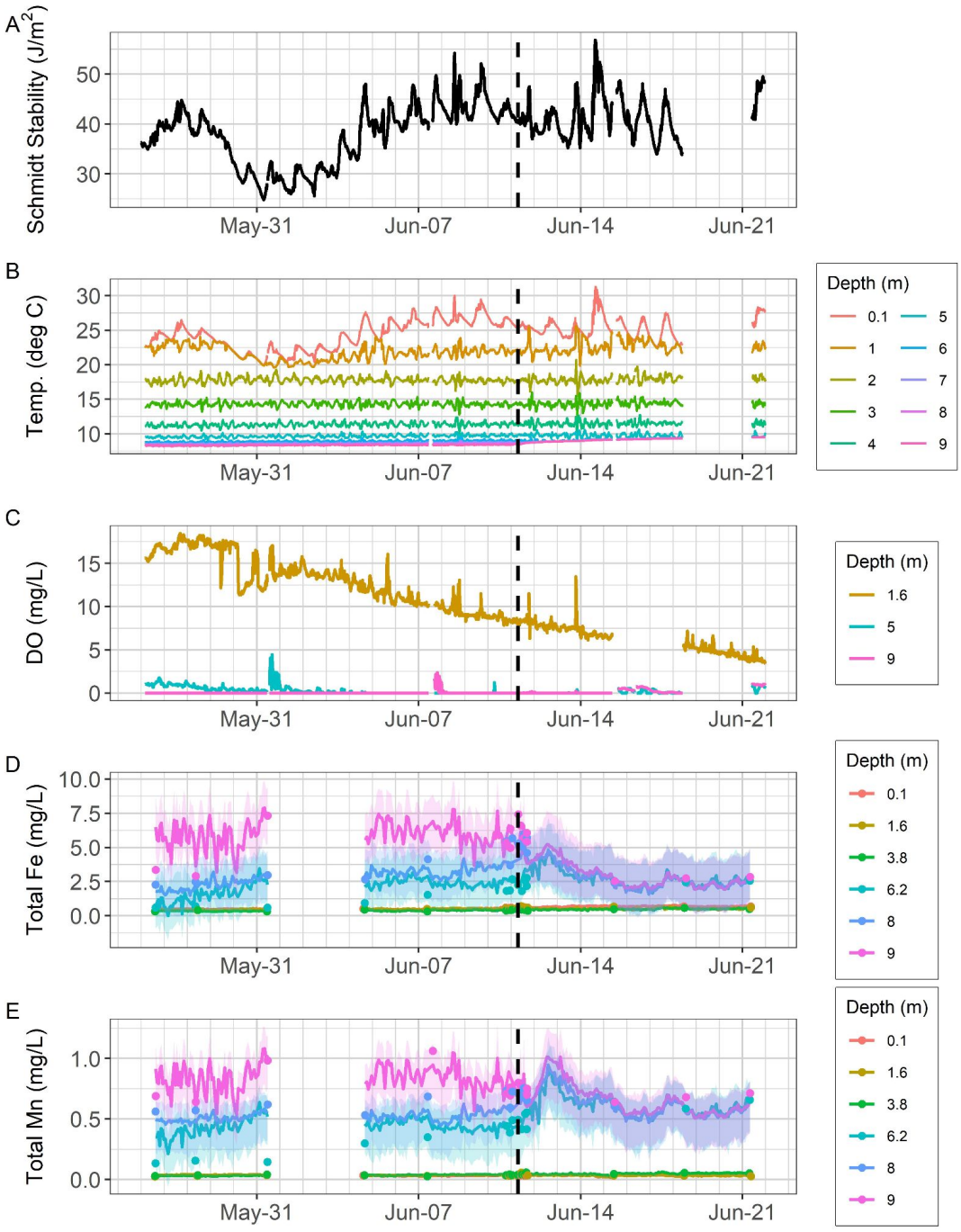

Figure 5. Time series plot of A) Schmidt stability, B) water temperature, C) dis-

solved oxygen, D) predicted total Fe concentrations (lines) with observed values (dots) and 90% predictive intervals (shaded area), and E) predicted total Mn concentrations (lines) with observed values (dots) and 90% predictive intervals (shaded areas) during the Oxygen On Deployment. The dashed vertical line represents the time that the HOx was turned on. Time series plots for soluble Fe and Mn are shown in Figure S17. Note that the MUX was not collecting data from 11:00 EDT 31 May 2021 until 14:30 EDT 4 June 2021 due to technical issues. Gaps in DO and water temperature data are due to sensor malfunction and/or maintenance.

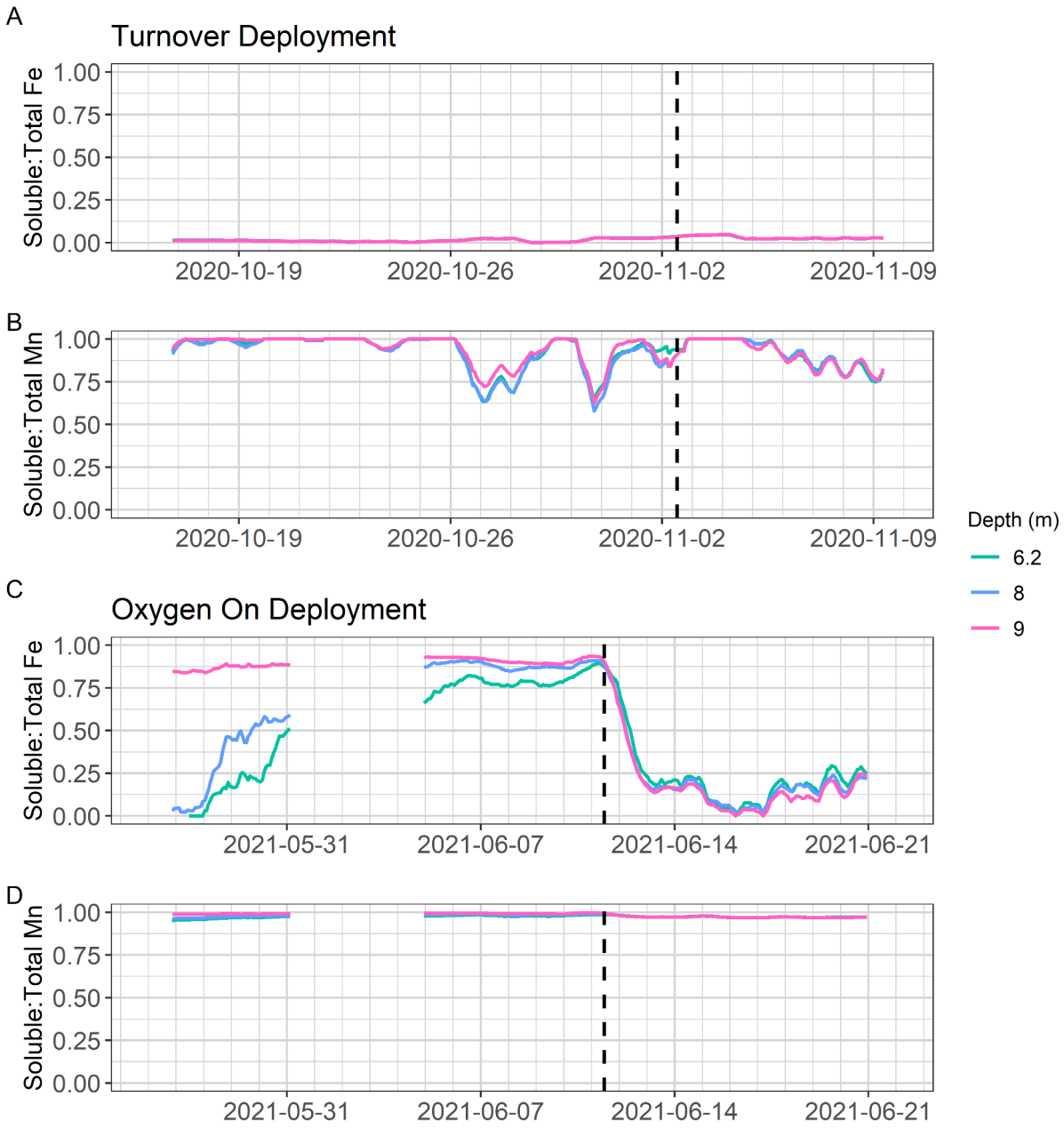

Figure 6: A) the ratio of predicted soluble Fe to total Fe and B) the ratio of predicted soluble Mn to total Mn in the hypolimnion during the Turnover deployment; C) the ratio of predicted soluble Fe to total Fe and D) the ratio of predicted soluble Mn to total Mn in the hypolimnion during the Oxygen On

Deployment. Values were smoothed with a 10-hr moving average to remove noise. The dashed vertical lines represent the times when reservoir turnover occurred in panels A-B and when the HOx system was turned on in panels C-D. PLSR predictions that had negative values were set to zero when calculating ratios and any ratio value that was greater than 1 was set to 1. Note that the MUX was not collecting data from 11:00 EDT 31 May 2021 until 14:30 EDT 4 June 2021 due to technical issues.

Table 1. Summary of PLSR model statistics. n = number of observations. Tot. = total, Sol. = soluble. Epi = epilimnion, Hypo = hypolimnion. The hypolimnetic soluble Fe PLSR models from the Turnover Deployment had a poor model fit due to the extremely low concentration range.

Variable	**Turnover Deployment**	**Oxygen On Deployment**			
	n	RMSEP (mg/L)	Adj. R^2	Components	Numb
Tot. Fe (Epi)	35	0.11	0.97	5	1
Tot. Fe (Hypo)	34	0.53	0.84	3	2
Sol. Fe (Epi)	35	0.02	0.74	5	1
Sol. Fe (Hypo)	34	0.06	0.06	3	2
Tot. Mn (Epi)	36	0.06	0.97	5	0
Tot. Mn (Hypo)	35	0.19	0.91	4	1
Sol. Mn (Epi)	35	0.06	0.96	5	1
Sol. Mn (Hypo)	35	0.22	0.90	3	1